Helix-Sense-Selective Encapsulation of Helical Poly(lactic acid)s within a Helical Cavity of Syndiotactic Poly(methyl methacrylate) with Helicity Memory

Tomoyuki Ikai,[†] Satoshi Kawabata,[†] Fumihiko Mamiya,[‡] Daisuke Taura,[†,‡] Naoki Ousaka,[†,‡,§] and Eiji Yashima*[†,‡]

[†]Department of Molecular and Macromolecular Chemistry, Graduate School of Engineering, Nagoya University, Chikusa-ku, Nagoya 464-8603, Japan.

[‡]Department of Molecular Design and Engineering, Graduate School of Engineering, Nagoya University, Chikusa-ku, Nagoya 464-8603, Japan.

ABSTRACT: We report a highly enantio- and helix-sense-selective encapsulation of helical poly(lactic acid)s (PLAs) through a unique "helix-in-helix" superstructure formation within the helical cavity of syndiotactic poly(methyl methacrylate) (st-PMMA) with a one-handed helicity memory, which enables the separation of the enantiomeric helices of the left (*M*)- and right (*P*)-handed-PLAs. The *M*- and *P*-helical PLAs with different molar masses and a narrow molar mass distribution were prepared by the ring-opening living polymerization of the optically-pure L- and D-lactides, respectively, followed by end-capping of the terminal residues of the PLAs with a 4-halobenzoate and then a C_{60} unit, giving the C_{60}-free and C_{60}-bound *M*- and *P*-PLAs. The C_{60}-free and C_{60}-bound *M*- and *P*-PLAs formed crystalline inclusion complexes with achiral st-PMMA accompanied by a preferred-handed helix induction in the st-PMMA backbone, thereby producing helix-in-helix superstructures with the same-handedness to each other. The induced helical st-PMMAs were retained after replacement with the achiral C_{60}, indicating the memory of the induced helicity of the st-PMMAs. Both the C_{60}-free and C_{60}-bound helical PLAs were enantio- and helix-sense selectively encapsulated into the helical hollow space of the optically-active *M*- and *P*-st-PMMAs with the helicity memory prepared using chiral amines. The *M*- and *P*-PLAs are preferentially encapsulated within the *M*- and *P*-st-PMMA helical cavity with the same-handedness to each other, respectively, independent of the terminal units. The C_{60}-bound PLAs were more efficiently and enantioselectively trapped in the st-PMMA compared to the C_{60}-free PLAs. The enantioselectivities were highly dependent on the molar mass of the C_{60}-bound and C_{60}-free PLAs, and significantly increased with the increasing molar mass of the PLAs.

INTRODUCTION

Biological polymers, such as polysaccharides (e.g., amylose and schizophyllan)[1-10] and assembled proteins[11-16] are known to possess a unique helical cavity or pore, within which a variety of small molecules and polymers are encapsulated in a size- and shape-selective manner, thereby producing discrete supramolecular inclusion complexes with specific functionalities that involve molecular/chiral recognition, catalysis, and ion/water transport.[9,17-21] Inspired by such biopolymer-based helical host systems, a large number of macrocyclic host molecules,[22-30] self-assembled organic/inorganic cages and capsules,[31-38] and helical foldamers[39-46] possessing a confined nano-space or cylindrical helical cavity suitable for encapsulating specific small molecules or oligomers has been extensively developed. However, because of their molecular-scale space, the encapsulating of polymers, in particular, helical polymers within their space or helical cavities is virtually impossible. Hence, the development of synthetic helical polymers with an optical activity showing an enantioselective or helix-sense-selective inclusion capability for helical polymers is an attractive challenge because of potential applications for separating enantiomers as chiral stationary phases (CSPs),[47] supramolecular liquid crystals,[6] and electronic and optoelectronic materials[2-9,18,48-55] as well as circularly polarized luminescence (CPL) when complexed with photoluminescent achiral polymers in a one-handed helical cavity.[56,57]

Previously, we found that syndiotactic poly(methyl methacrylate) (st-PMMA), a commodity plastic widely used as plastic optical fibers,[58] folds into either an excess left (*M*)- or right (*P*)-handed 18_1-helical conformation (18 monomer units per one turn) assisted by an optically-active alcohol or amine in toluene upon gelation, thus creating a helical cavity of about 1 nm in diameter,[59-62] in which achiral and chiral fullerenes can be encapsulated in a size- and/or enantio-selective manner through an induced-fit mechanism,[59,61,63-65] thereby producing unique peapod-like inclusion complexes with an optical activity that are retained (memorized) after complete removal of the chiral additives.[59-62] Such a one-handed helical cavity of the st-PMMA with a helicity memory is self-adjustable while maintaining its helical handedness, thus allowing the helix-sense-selective encapsulation of the complementary isotactic PMMA (it-PMMA) to produce the first optically-active PMMA stereocomplex[60] composed of an inner it-PMMA double-helix

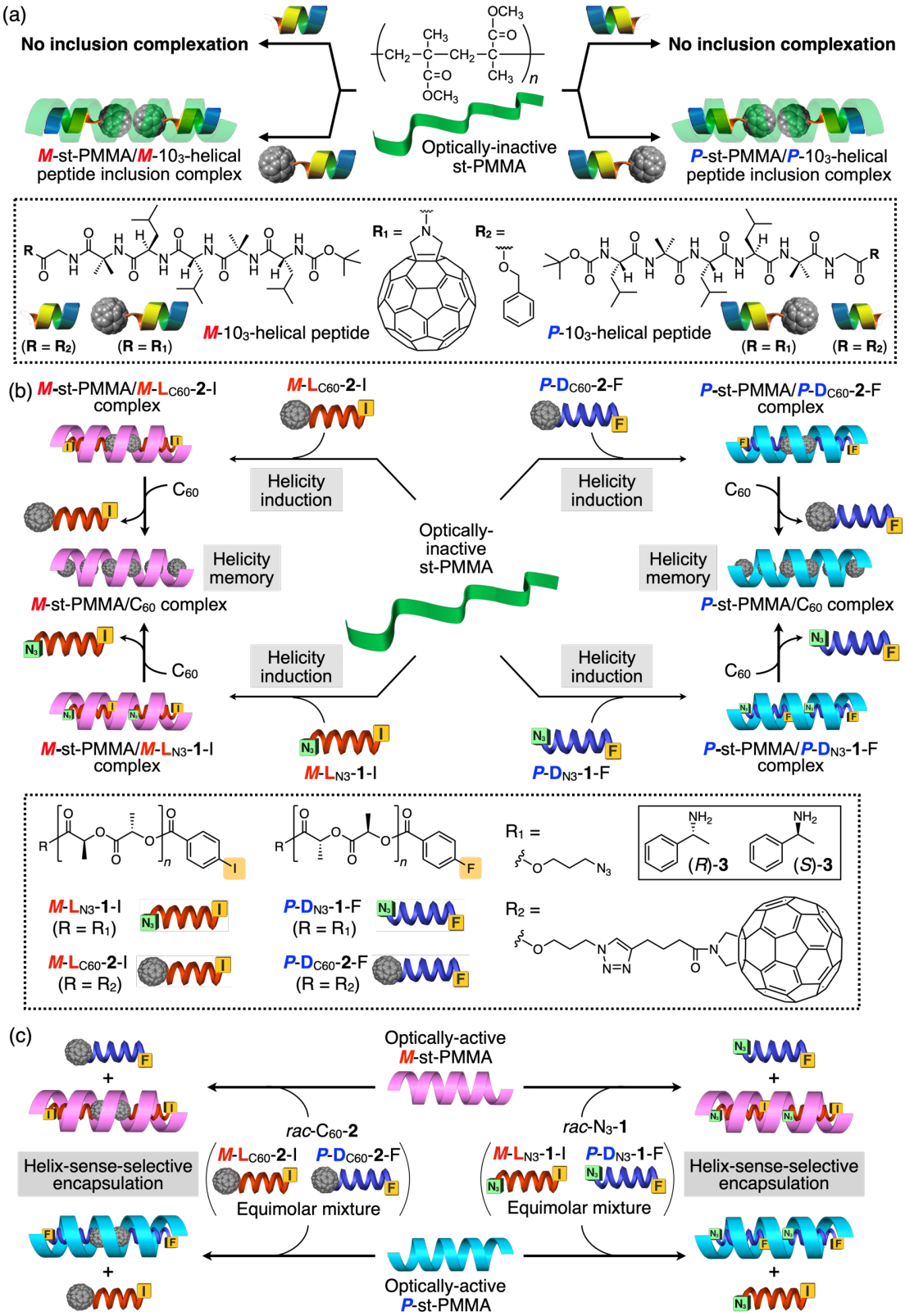

Figure 1. (a) Schematic illustration of the "helix-in-helix" superstructure formation through encapsulation of C_{60}-bound *M*- and *P*-10_3-helical peptides within the st-PMMA helical cavity.[75] (b) Structures of C_{60}-bound (***M***-**L**$_{C60}$-**2**-I and ***P***-**D**$_{C60}$-**2**-F) and C_{60}-free (***M***-**L**$_{N3}$-**1**-I and ***P***-**D**$_{N3}$-**1**-F) *M*- and *P*-helical PLAs and optically-active amines ((*R*)- and (*S*)-**3**) and a schematic illustration of the macromolecular helicity induction in st-PMMA upon inclusion complex formations with the C_{60}-bound and C_{60}-free *M*- and *P*-helical PLAs and subsequent memory of the induced macromolecular helicities of st-PMMA by replacing the encapsulated *M*- and *P*-helical PLAs with the achiral C_{60}. (c) Helix-sense-selective encapsulation of C_{60}-bound and C_{60}-free *M*- and *P*-helical PLAs within a helical cavity of st-PMMA with a one-handed helicity memory based on the "helix-in-helix" superstructure formation.

Scheme 1. Synthesis of the C_{60}-Free (*M*-L_{N3}-1**-I and *P*-D_{N3}-**1**-F) and C_{60}-Bound (*M*-L_{C60}-**2**-I and *P*-D_{C60}-**2**-F) Optically-Active Polylactides**

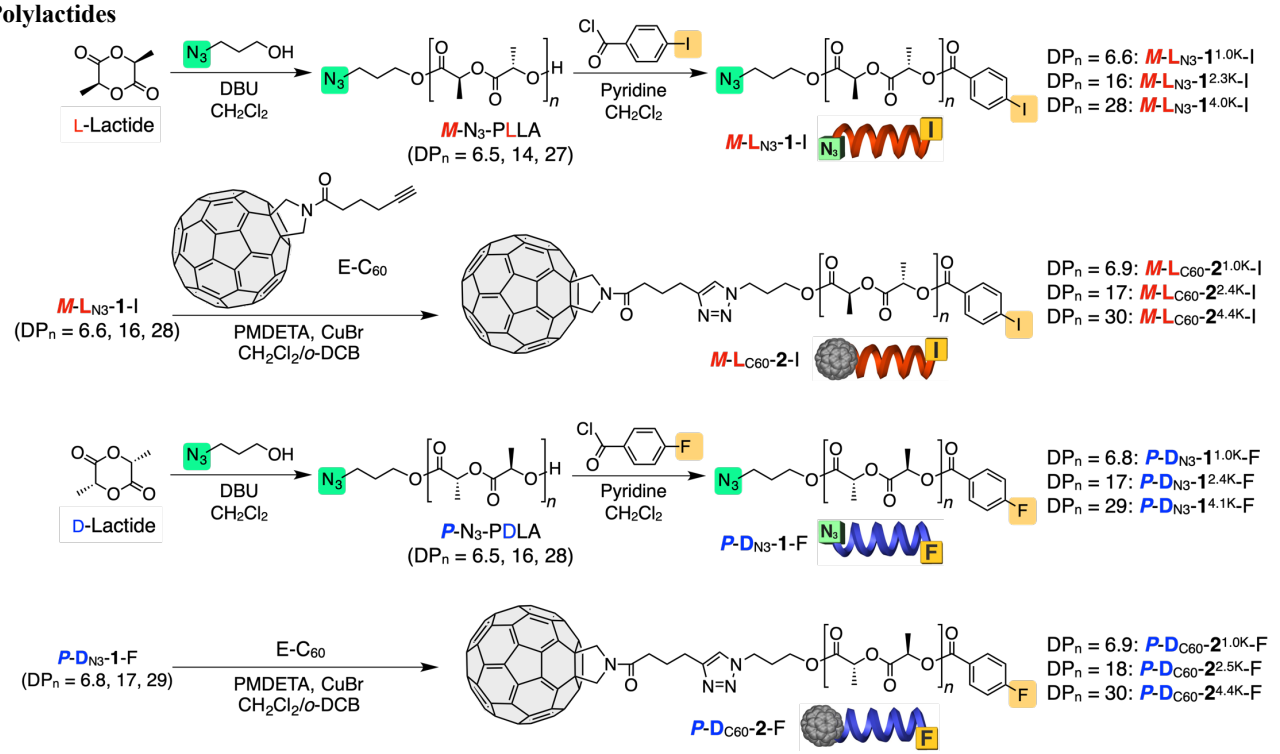

surrounded by the st-PMMA single-helix with the same handedness to each other.[66-74]

Taking advantage of the specific interactions between fullerenes and the hydrophobic helical cavity of st-PMMA, we recently succeeded in the construction of a unique "helix-in-helix" superstructure through encapsulation of the *M*- and *P*-10_3-helical peptides (Figure 1a) within the st-PMMA helical cavity when a C_{60} moiety was introduced at one end of the peptides, through which a preferred-handed helix with the same-handedness as that of the encapsulated peptide was, at the same time, induced in the st-PMMA backbone.[75] Of particular importance is the terminal C_{60} unit of the peptides that is essential for the inclusion complex formation with the st-PMMA or no inclusion complexation took place. The results imply that a C_{60} unit can serve as a molecular carrier or transporter of particular organic molecules and polymers into the helical cavity of the st-PMMA once introduced at their terminals, resulting in unique supramolecular inclusion complexes.[76]

We envisioned that poly(lactic acid) (PLA), one of the popular bio-based, biocompatible, and biodegradable polyesters,[77] would also be encapsulated in the st-PMMA helical cavity once the PLA is end-capped with a C_{60} unit because the homochiral PLAs, namely, poly(L-lactic acid) (PLLA) and poly(D-lactic acid) (PDLA) take *M*- and *P*-10_3-helical structures, respectively,[78-80] which resemble the helical polypeptides, specifically, poly(D- or L-alanine).[81,82] We now report the unprecedented helix-sense-selective encapsulation of C_{60}-bound *M*- and *P*-helical PLAs (***M***-C_{60}-**L-2**-I and ***P***-C_{60}-**D-2**-F) (Scheme 1 and Figure 1b) within the helical cavity of the preferred-handed helical st-PMMA prepared by the helicity induction and memory strategy[42,59-62] using chiral amines, such as (*R*)- and (*S*)-1-phenylethylamine ((*R*)- and (*S*)-**3**),[61,62] based on a unique "helix-in-helix" superstructure formation, which would enable us to separate the enantiomeric helices of PLAs (Figure 1c). The separation of enantiomers of optically-active polymers, in particular, helical polymers, is quite rare.[83-85] Although chiral recognition of the enantiomeric helical PLAs has been reported using cyclodextrins[86] and amylose,[87,88] the *M*- and *P*-helical PLAs were neither separated nor isolated, providing little information about the enantioselective inclusion complex formation at a molecular level as well as its enantioselectivity (helix-sense selectivity). During the course of our studies, we surprisingly found that the C_{60}-free *M*- and *P*-helical PLAs (***M***-N_3-**L-1**-I and ***P***-N_3-**D-1**-F) (Scheme 1 and Figure 1b) prepared as precursors for the C_{60}-bound *M*- and *P*-helical PLAs are also helix-sense selectively included in the st-PMMA helical nanotube, resulting in a similar "helix-in-helix" superstructure. The effects of the end-capped C_{60} unit and molar mass of the PLAs on the helix-sense-selective inclusion complexations in the st-PMMA helical nanotube with a helicity memory and their preferred-handed helix induction abilities to the optically-inactive st-PMMA (Figure 1b,c) are also investigated.

RESULTS AND DISCUSSION

Synthesis and Characterization of C_{60}-Free and C_{60}-Bound *M*- and *P*-Helical PLAs. The C_{60}-free (N_3-**1**) and C_{60}-bound *M*-L- and *P*-D-helical PLAs (C_{60}-**2**) with different molar masses and a narrow molar mass distribution were synthesized according to Scheme 1. The ring-opening living polymerization of the optically-pure L- and D-lactides (enantiomeric excess (ee) > 99% (Figure S1)) initiated with 3-azido-1-propanol in the presence of 1,8-diazabicyclo[5.4.0]-7-undecene (DBU) as a catalyst (Table S1),[89] followed by esterification of the terminal hydroxy groups using 4-iodo- and 4-fluorobenzoyl chlorides, respectively, afforded the C_{60}-free *M*- and *P*-helical PLAs (***M***-L_{N3}-**1**-I and ***P***-D_{N3}-**1**-F) (Table S2). The copper(I)-catalyzed click reaction of the resulting PLAs bearing an azido residue (***M***-L_{N3}-**1**-I and ***P***-D_{N3}-**1**-F) with an alkyne-terminated C_{60} derivative (E-C_{60}) produced the C_{60}-bound *M*- and *P*-helical

Table 1. Characteristics of PLA Prepolymers and C_{60}-Free and C_{60}-Bound *M*- and *P*-PLAs

entry	sample code	$M_{n,SEC}$ (10^3) [a]	M_w/M_n [a]	$M_{n,NMR}$ (10^3) [b]	$DP_{n,NMR}$ [c]	$f_{end\ group}$ (%) [d]	T_m (°C) [e]
1	***M*-N_3-PLLA$^{0.9K}$**	1.53	1.26	0.94	6.5	–	92
2	***M*-N_3-PLLA$^{2.1K}$**	3.55	1.11	2.08	14	–	130
3	***M*-N_3-PLLA$^{3.9K}$**	6.28	1.11	3.85	27	–	151
4	***M*-$\mathbf{L}_{N3}$-$\mathbf{1}^{1.0K}$-I**	1.61	1.19	0.95	6.6	>99	96
5	***M*-$\mathbf{L}_{N3}$-$\mathbf{1}^{2.3K}$-I**	4.14	1.11	2.30	16	>99	137
6	***M*-$\mathbf{L}_{N3}$-$\mathbf{1}^{4.0K}$-I**	6.53	1.12	4.01	28	>99	149
7	***M*-$\mathbf{L}_{C60}$-$\mathbf{2}^{1.0K}$-I**	1.82	1.24	0.99	6.9	>99	–[f]
8	***M*-$\mathbf{L}_{C60}$-$\mathbf{2}^{2.4K}$-I**	4.38	1.20	2.43	17	>99	141
9	***M*-$\mathbf{L}_{C60}$-$\mathbf{2}^{4.4K}$-I**	7.73	1.32	4.36	30	>99	146
10	***P*-N_3-PDLA$^{0.9K}$**	1.40	1.31	0.94	6.5	–	93
11	***P*-N_3-PDLA$^{2.3K}$**	3.82	1.12	2.28	16	–	136
12	***P*-N_3-PDLA$^{4.0K}$**	7.11	1.12	4.04	28	–	152
13	***P*-$\mathbf{D}_{N3}$-$\mathbf{1}^{1.0K}$-F**	1.62	1.23	0.98	6.8	>99	95
14	***P*-$\mathbf{D}_{N3}$-$\mathbf{1}^{2.4K}$-F**	4.15	1.11	2.41	17	>99	138
15	***P*-$\mathbf{D}_{N3}$-$\mathbf{1}^{4.1K}$-F**	7.38	1.12	4.11	29	>99	149
16	***P*-$\mathbf{D}_{C60}$-$\mathbf{2}^{1.0K}$-F**	1.63	1.41	1.00	6.9	>99	–[f]
17	***P*-$\mathbf{D}_{C60}$-$\mathbf{2}^{2.5K}$-F**	4.75	1.26	2.52	18	>99	141
18	***P*-$\mathbf{D}_{C60}$-$\mathbf{2}^{4.4K}$-F**	7.93	1.35	4.39	30	>99	146

[a] Estimated by SEC (polystyrene standards) with $CHCl_3$ as the eluent. [b] Determined by the ^{1}H NMR end-group analysis in $CDCl_3$. [c] Number-average degree of polymerization determined by $M_{n,NMR}$. [d] Functionality of the end-capped benzoate (entries 4–6 and 13–15) or C_{60} (entries 7–9 and 16–18) residue estimated by ^{1}H NMR in $CDCl_3$. [e] Melting point determined by DSC. [f] Not observed in the DSC thermogram.

PLAs (***M*-$\mathbf{L}_{C60}$-**2**-I and ***P*-$\mathbf{D}_{C60}$-**2**-F) in good yields (Table S3). The different terminal benzoate groups were introduced to the C_{60}-free and C_{60}-bound *M*-L- and *P*-D-helical PLAs to determine the ee of the nonracemic **1** and **2** by ^{1}H NMR spectroscopy after enantioselective extractions, respectively (see below (Figure 6a) and the Supporting Information (SI)), since the C_{60}-bound and C_{60}-free L- and D-PLA enantiomers could not be separated by chiral HPLC.

The polymerization results of the L- and D-lactides and characteristics of the PLA prepolymers and the C_{60}-free and C_{60}-bound *M*- and *P*-helical PLAs are summarized in Table 1. The structures were fully characterized and identified using size exclusion chromatography (SEC), NMR and IR spectroscopies, and matrix-assisted laser desorption-ionization time-of-flight mass (MALDI-TOF-MS) measurements (see the Experimental Section in the SI and Figures 2 and S2–S6). The number-average molar masses ($M_{n,NMR}$) of the PLA chains and the functionalities ($f_{end\ group}$) of the 4-iodo- or 4-fluorobenzoate ($f_{benzoate}$) and C_{60} (f_{C60}) of the isolated C_{60}-free and C_{60}-bound PLAs were estimated based on the ^{1}H NMR end group analyses, showing the almost complete functionalizations of the PLA terminal ends, which were further supported by the MALDI-TOF-MS measurements. The MALDI-TOF-MS spectra of a series of ***M*-N_3-PLLA and ***P*-N_3-PDLA with different $M_{n,NMR}$ values before and after end-capping with 4-iodo- or 4-fluorobenzoyl chloride followed by C_{60} showed one main series of peaks, whose intervals were regular and separated by approximately 144.0 (*m*/*z*) mass corresponding to the molar mass of the lactic acid monomer; each molecular peak equals the molecular mass expected for the as-prepared PLAs (***M*-N_3-PLLA and ***P*-N_3-PDLA) end-capped with 4-iodo- or 4-fluorobenzoate (***M*-$\mathbf{L}_{N3}$-**1**-I and ***P*-$\mathbf{D}_{N3}$-**1**-F) and further with C_{60} (***M*-$\mathbf{L}_{C60}$-**2**-I and ***P*-$\mathbf{D}_{C60}$-**2**-F) (Figures 2b and S2–S6). Sample codes are abbreviated using the helicity of PLA (*M* or *P*), the absolute configuration of the lactide (L or D), $M_{n,NMR}$, and the end groups such that ***M*-$\mathbf{L}_{C60}$-$\mathbf{2}^{1.0K}$-I, for example, stands for the *M*-PLLA end-capped with 4-iodobenzoate and C_{60} with the $M_{n,NMR}$ of the PLA chain (ca. 1.0 K) (Scheme 1 and Table 1).

The st-PMMA was synthesized using the stereospecific polymerization technique (see SI).[90] The M_n, its distribution (M_w/M_n), and stereoregularities (*mm* : *mr* : *rr*) were as follows: M_n = 616 kDa, M_w/M_n = 1.36, and *mm* : *mr* : *rr* = 0 : 4 : 96, in which *m* and *r* represent the isotactic (it) and st dyads of the meso and racemo sequences, respectively, and *mm*, *mr*, and *rr* are the corresponding triad sequences.

Inclusion Complex Formation of C_{60}-Bound and C_{60}-Free PLAs with st-PMMA. As reported previously,[59] the st-PMMA/C_{60} complex gels in toluene were completely dissolved to form homogeneous solutions by heating above 90 °C, in which st-PMMA and C_{60} molecules are molecularly dispersed. Based on this observation, the encapsulation experiments of PLAs with st-PMMA were performed in toluene at 110 °C. As anticipated, the C_{60}-bound PLAs (***M*-$\mathbf{L}_{C60}$-**2**-I and ***P*-$\mathbf{D}_{C60}$-**2**-F) were efficiently encapsulated within the st-PMMA helical cavity during gelation of an optically-inactive st-PMMA in toluene upon heating at 110 °C, followed by cooling to room temperature (Figure 3a),[59-62,75] which was almost independent

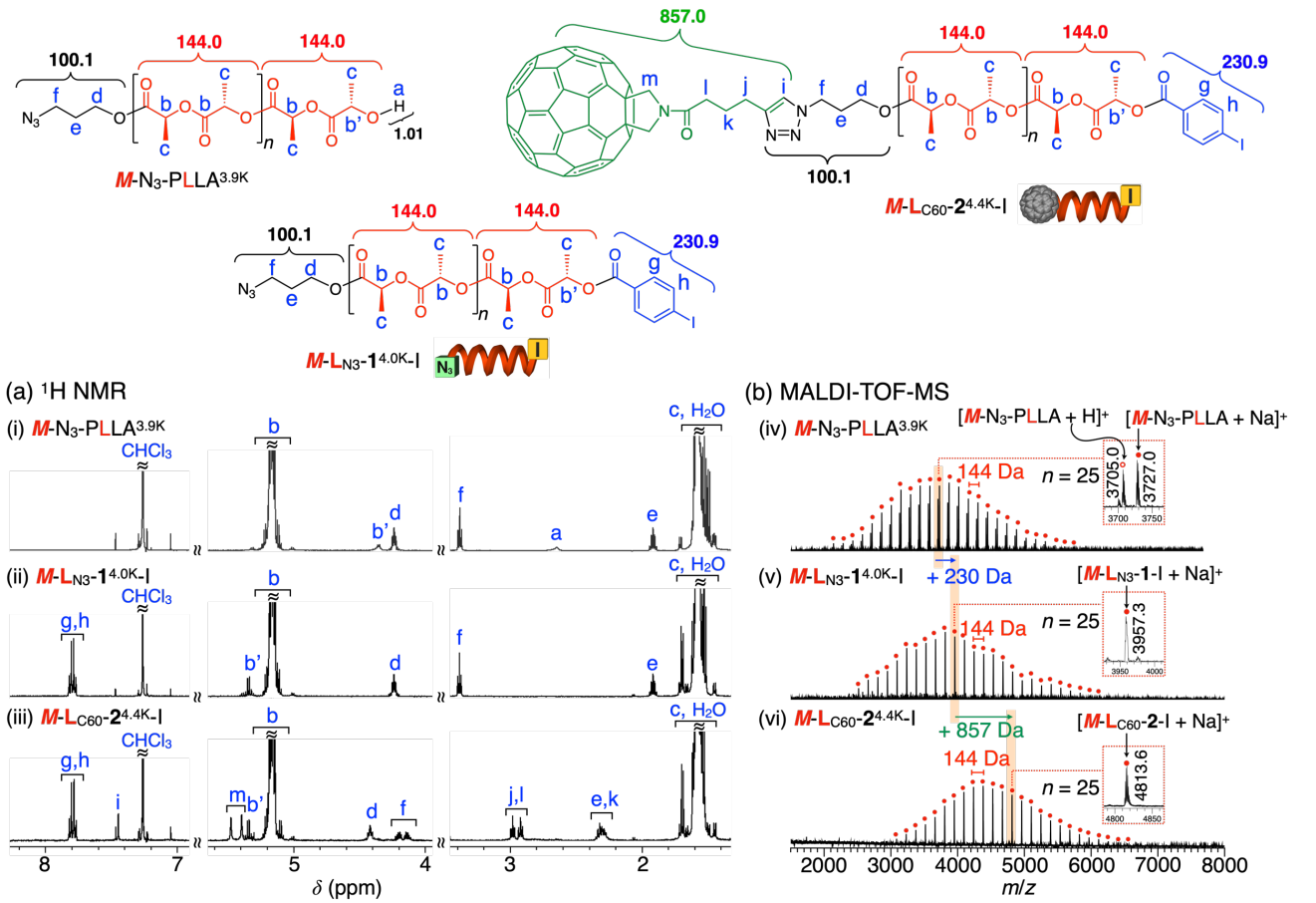

Figure 2. (a) ^{1}H NMR and (b) MALDI-TOF-MS spectra of ***M***-N_3-PLLA$^{3.9K}$, ***M***-$\mathbf{L}_{N3}$-$\mathbf{1}^{4.0K}$-I, and ***M***-$\mathbf{L}_{C60}$-$\mathbf{2}^{4.4K}$-I. The NMR spectra were measured in $CDCl_3$ at 25 °C and the MS measurements were performed using dithranol as a matrix and sodium iodide as a cationizing agent.

of the $M_{n,NMR}$ of **2**. Typically, st-PMMA (10 mg) was dissolved in a toluene solution of ***M***-$\mathbf{L}_{C60}$-$\mathbf{2}^{4.4K}$-I (3.0 mg/mL, 1.0 mL) at 110 ºC. After the solution was cooled to room temperature, the solution gelled within 10 min (Figure 3a, middle). The resulting soft gel was then centrifuged at 1700 *g* for 10 min (Figure 3a, right) and the supernatant containing the unencapsulated ***M***-$\mathbf{L}_{C60}$-$\mathbf{2}^{4.4K}$-I was removed from the gel by decantation. The amount of the ***M***-$\mathbf{L}_{C60}$-$\mathbf{2}^{4.4K}$-I encapsulated in the st-PMMA was estimated based on the differences in the absorption spectra between the feed ***M***-$\mathbf{L}_{C60}$-$\mathbf{2}^{4.4K}$-I and the supernatant (Figure S7) according to a previously reported method (see Section 3 in the SI).[75] The inclusion complex formation results are summarized in Table 2. The encapsulated C_{60}-bound **2** content increased by using a higher concentrated C_{60}-bound **2** solution in toluene (>9.0 mg/mL) as the feed and reached an almost maximum value of ca. 24 wt% (run 5, Table 2).

The "helix-in-helix" superstructured inclusion complex formations were confirmed by differential scanning calorimetry (DSC) and X-ray diffraction (XRD) measurements of the st-PMMA complexed with C_{60}-bound **2** films containing about 15 wt% of C_{60}-bound **2** prepared from the gels, which revealed a crystalline structure of the st-PMMA/C_{60}-bound **2** complexes (Figure 3c,d and Table 2) as supported by an apparent melting temperature (T_m) (ca. 180 °C) and a characteristic reflection at the *d*-spacing of ca. 1.8 nm due to the bundle structures of the helical st-PMMA chains, which are almost independent of the $M_{n,NMR}$ of **2**; the observed *d*-spacing is larger than that of the st-PMMA complexed with C_{60} (1.67 nm), but smaller than that with larger fullerenes, such as C_{70} (1.92 nm) and C_{84} (2.04 nm),[59] and is almost identical to that with the C_{60}-bound *P*-L-peptide (Figure 1a) (1.80 nm).[75] We also found that significant differences were not observed in the T_m and *d*-values when the encapsulated C_{60}-bound **2** content in the st-PMMA increased to 23.5 wt% (run 5, Table 2 and Figure S8). Contrary to our expectation, the C_{60}-free PLA (***M***-$\mathbf{L}_{N3}$-$\mathbf{1}^{4.0K}$-I) was also found to form an inclusion complex with st-PMMA in toluene by heating followed by cooling to room temperature, resulting in gelation (Figure 3b). Compared with the previously reported C_{60}-free 10_3-helical peptides that could not form an inclusion complex with st-PMMA,[75] the PLA chains with the same helical geometry seem to more compatibly fit the helical cavities of the st-PMMA, leading to a larger enthalpy gain that mostly overcomes the entropic loss. The st-PMMA/C_{60}-free **1** inclusion complex film showed a slightly lower T_m value (174 °C) but a similar *d*-value (1.86 nm) as those of the st-PMMA/C_{60}-bound **2** complexes (Figure 3c–e and Table 2). St-PMMA has been suggested to form a crystalline stereocomplex only with its complementary it-PMMA since its discovery in 1958.[91-93] Hence, the present finding will provide a rare opportunity for applications of the crystalline st-PMMA/PLA complexes as a practically useful hybrid plastic composed of biodegradable PLAs.

Preferred-Handed Helix Formation in st-PMMA Induced by C_{60}-Bound and C_{60}-Free *M*- and *P*-PLAs. We anticipated that the one-handed helical C_{60}-bound and C_{60}-free *M*- and *P*-PLAs could induce one of the helices in st-PMMA once

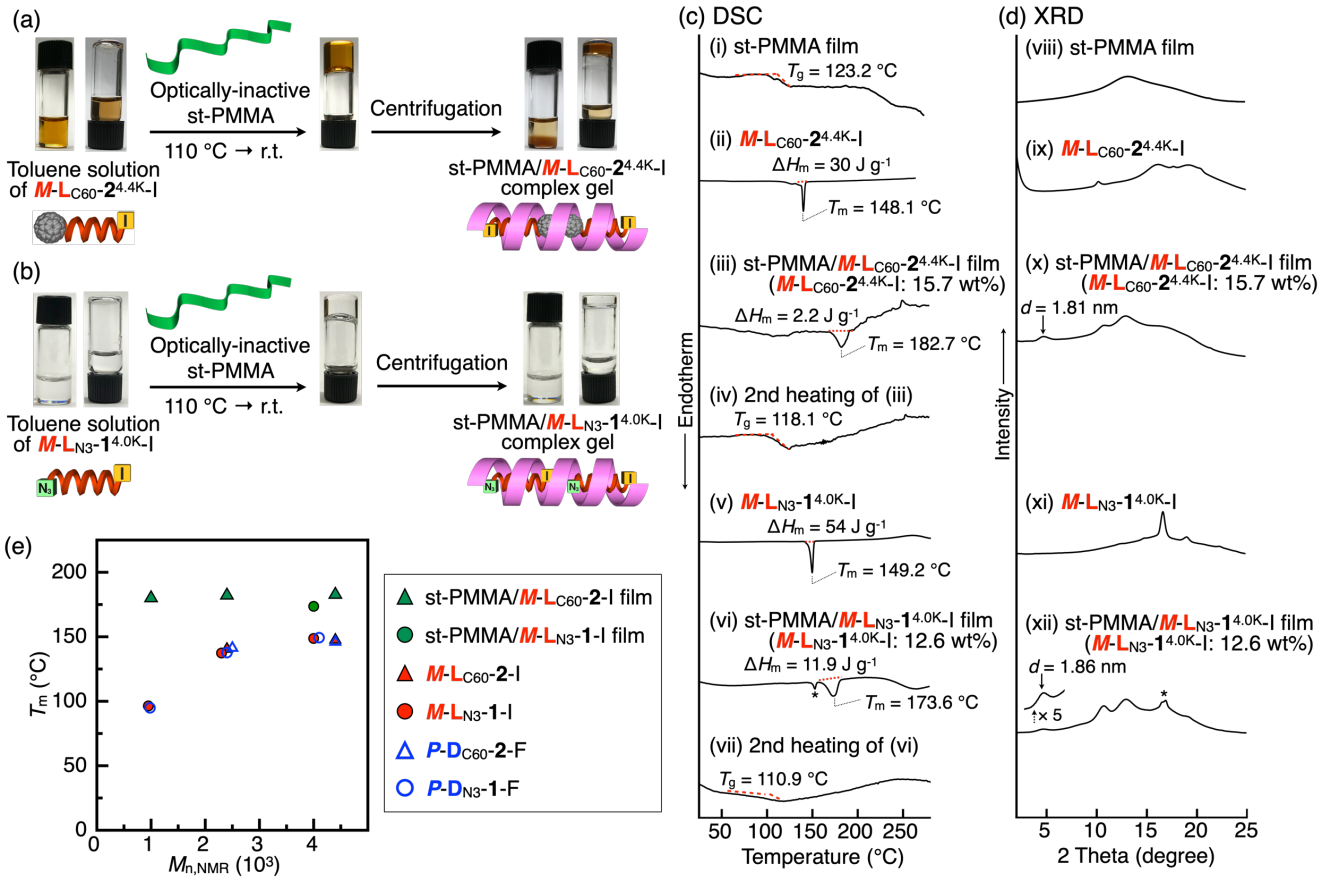

Figure 3. (a, b) Photographs of toluene solutions of ***M*-L**$_{C60}$-**2**$^{4.4K}$-I (a; 3.0 mg/mL, 1.0 mL; left) and ***M*-L**$_{N3}$-**1**$^{4.0K}$-I (b; 14.5 mg/mL, 0.80 mL; left), st-PMMA/***M*-L**$_{C60}$-**2**$^{4.4K}$-I (a) and st-PMMA/***M*-L**$_{N3}$-**1**$^{4.0K}$-I (b) gels after the addition of st-PMMA (10 mg (a) and 8 mg (b), respectively) with subsequent heating to 110 °C and then cooling to room temperature (middle), and the st-PMMA/***M*-L**$_{C60}$-**2**$^{4.4K}$-I (a) and st-PMMA/***M*-L**$_{N3}$-**1**$^{4.0K}$-I (b) complex gels after centrifugation at 1700 *g* for 10 min (right). (c) DSC thermograms of st-PMMA (i), ***M*-L**$_{C60}$-**2**$^{4.4K}$-I (ii), st-PMMA/***M*-L**$_{C60}$-**2**$^{4.4K}$-I complex film containing 15.7 wt% of ***M*-L**$_{C60}$-**2**$^{4.4K}$-I (iii), ***M*-L**$_{N3}$-**1**$^{4.0K}$-I (v), and st-PMMA/***M*-L**$_{N3}$-**1**$^{4.0K}$-I complex film containing 12.6 wt% of ***M*-L**$_{N3}$-**1**$^{4.0K}$-I (vi). These films were prepared by evaporating the solvents from the st-PMMA and st-PMMA/PLA complex gels in toluene. The DSC measurements were conducted after cooling the samples at –20 °C, followed by heating to 280 °C (10 °C/min) under nitrogen. The samples (iii) and (vi) were then cooled to –20 °C (40 °C/min), and then heated again ((iv) and (vii), respectively; 10 °C/min). The arrow to the left of the DSC data indicates the endothermic direction. Asterisk (*) in (vi) denotes the melting peak from the free ***M*-L**$_{N3}$-**1**$^{4.0K}$-I. (d) XRD profiles of st-PMMA (viii), ***M*-L**$_{C60}$-**2**$^{4.4K}$-I (ix), st-PMMA/***M*-L**$_{C60}$-**2**$^{4.4K}$-I complex film (15.7 wt%) (x), ***M*-L**$_{N3}$-**1**$^{4.0K}$-I (xi), and st-PMMA/***M*-L**$_{N3}$-**1**$^{4.0K}$-I complex film (12.6 wt%) (xii). Asterisk (*) in (xii) denotes the diffraction peak from the free ***M*-L**$_{N3}$-**1**$^{4.0K}$-I. (e) Plots of melting temperature (T_m) of st-PMMA/PLAs complex films and PLAs versus the number-average molar mass of PLAs.

encapsulated in the st-PMMA helical cavity (Figure 1b), as observed for the inclusion complex formation with the C_{60}-bound *M*-D- and *P*-L-peptides.[75] In fact, the st-PMMA gels complexed with C_{60}-bound *M*- and *P*-C_{60}-**2** (15.6 – 18.5 wt%) showed mirror-image electric circular dichroism (ECD) and vibrational CD (VCD) spectra in the achiral fullerene chromophore and PMMA IR regions in toluene and toluene-d_8, respectively (Figures 4d,e and S9f–i), while the C_{60}-bound PLAs (C_{60}-**2**) themselves exhibited negligibly weak ECD signals in the achiral fullerene chromophore regions in toluene-d_8 (Figures 4a and S9b,c). The C_{60}-free *M*- and *P*-PLAs (N_3-**1**) also induced an excess of the one helical sense in st-PMMA, thus showing VCD signals in the PMMA IR regions (Figure 4f), which were different from those of the C_{60}-free *M*- and *P*-PLAs (N_3-**1**) (Figure 4c). The observed VCD spectral patterns of the st-PMMAs complexed with C_{60}-bound and C_{60}-free *M*- and *P*-PLAs agree well with those of the calculated *M*- and *P*-18_1-helical st-PMMAs, respectively (Figure 4g), thereby producing the helix-in-helix superstructures with the same-handedness to each other.[60,75] The inclusion complex structures of *M*-st-PMMA with C_{60}-bound and C_{60}-free *M*-PLAs optimized by molecular mechanics calculations based on an 18_1-helical st-PMMA structure[66] support the helix-in-helix superstructures, in which the encapsulated C_{60}-bound and C_{60}-free *M*-PLAs fill the st-PMMA helical nanotube, while maintaining its 10_3-helical structures (Figure S10).[78-80] The molecular arrangements of the C_{60}-bound and C_{60}-free *M*-PLAs within the st-PMMA helical cavity are not clear at present, but preferable stacking interactions between the C_{60} units of the C_{60}-bound-PLAs[59,75,94,95] may suggest a head-to-head packing array that may exist in part. The VCD intensities of the st-PMMAs induced by the C_{60}-bound and C_{60}-free *M*- and *P*-PLAs were relatively weaker than those induced by the (*R*)- and (*S*)-**3**[62] and C_{60}-bound *P*-L- and *M*-D-10_3-helical peptides.[75]

Interestingly, the encapsulated C_{60}-bound and C_{60}-free PLAs in the st-PMMA cavities could be almost completely replaced by the achiral C_{60} as evidenced by the difference in the absorption and/or NMR spectra before and after the

replacement (Figures 1b and S12) due to a higher affinity of st-PMMA to C_{60} over the C_{60}-bound and C_{60}-free PLAs. More interestingly, the preferred-handed helical structures of the st-PMMAs induced by the C_{60}-bound and C_{60}-free *M*- and *P*-PLAs were retained after replacement by the achiral C_{60}, thus showing apparent ECDs in the C_{60} chromophore regions (Figure 5a), which were completely different from those of the st-PMMA complexed with *M*- and *P*-C_{60}-bound PLAs (Figure 4d), but were similar in their patterns to those of the st-PMMA/C_{60} complexes prepared from the isolated optically-active *M*- and *P*-st-PMMAs complexed with C_{60},[59,62] indicating that the induced helical conformations of the st-PMMAs were memorized after the *M*- and *P*-C_{60}-bound and C_{60}-free PLAs were replaced by the achiral C_{60}.[59,60,62] The ECD intensities of the helicity-memorized *M*- and *P*-st-PMMA/C_{60} complexes were almost identical and independent of the terminal groups (C_{60} or azido group) of the PLA chains when the amounts of the encapsulated *M*- and *P*-PLA chains are the same (Figure 5b(ii–v)), indicating that the helical chirality of the *M*- and *P*-PLA chains play a dominant role to induce the preferred-handed helical conformation in st-PMMA. The ECD intensity of the helicity-memorized st-PMMA complexed with C_{60} tended to increase with an increase in the amount of the C_{60}-bound and C_{60}-free *M*- and *P*-PLAs encapsulated in the st-PMMA helical cavity during the helicity induction process (Figures 5b(i,ii) and S13).

Table 2. Characteristics of Inclusion Complexes of C_{60}-Bound and C_{60}-Free *M*- and *P*-PLAs with st-PMMA [a]

run	PLA	st-PMMA/PLA inclusion complex		
		encapsulated PLA (wt%) [b]	*d* (nm) [c]	T_m (°C) [d]
1	***M*-L$_{C60}$-2$^{1.0K}$-I**	15.2	1.77	180
2	***M*-L$_{C60}$-2$^{2.4K}$-I**	15.3	1.82	181
3	***M*-L$_{C60}$-2$^{4.4K}$-I**	15.7	1.81	183
4	***P*-D$_{C60}$-2$^{4.4K}$-F**	16.8	–	–
5	***M*-L$_{C60}$-2$^{4.4K}$-I**	23.5	1.86	181
6	***M*-L$_{N3}$-1$^{4.0K}$-I**	12.6	1.86	174

[a] The st-PMMA/PLA complex gels were prepared by adding a toluene (runs 1–5) or toluene-d_8 (run 6) solution of PLA (3.0 mg/mL, 1.0 mL in runs 1–4, 9.0 mg/mL, 0.40 mL in run 5, and 14.5 mg/mL, 0.80 mL in run 6) to st-PMMA (10.0 mg in runs 1–4, 4.0 mg in run 5, and 8.0 mg in run 6) followed by heating to 110 °C and cooling to room temperature, and then centrifuged. [b] Determined by absorption (runs 1–5) and ^{1}H NMR (run 6) analyses. [c] Estimated by XRD of the st-PMMA/PLA complex films. [d] Melting point determined by DSC of the st-PMMA/PLA complex films.

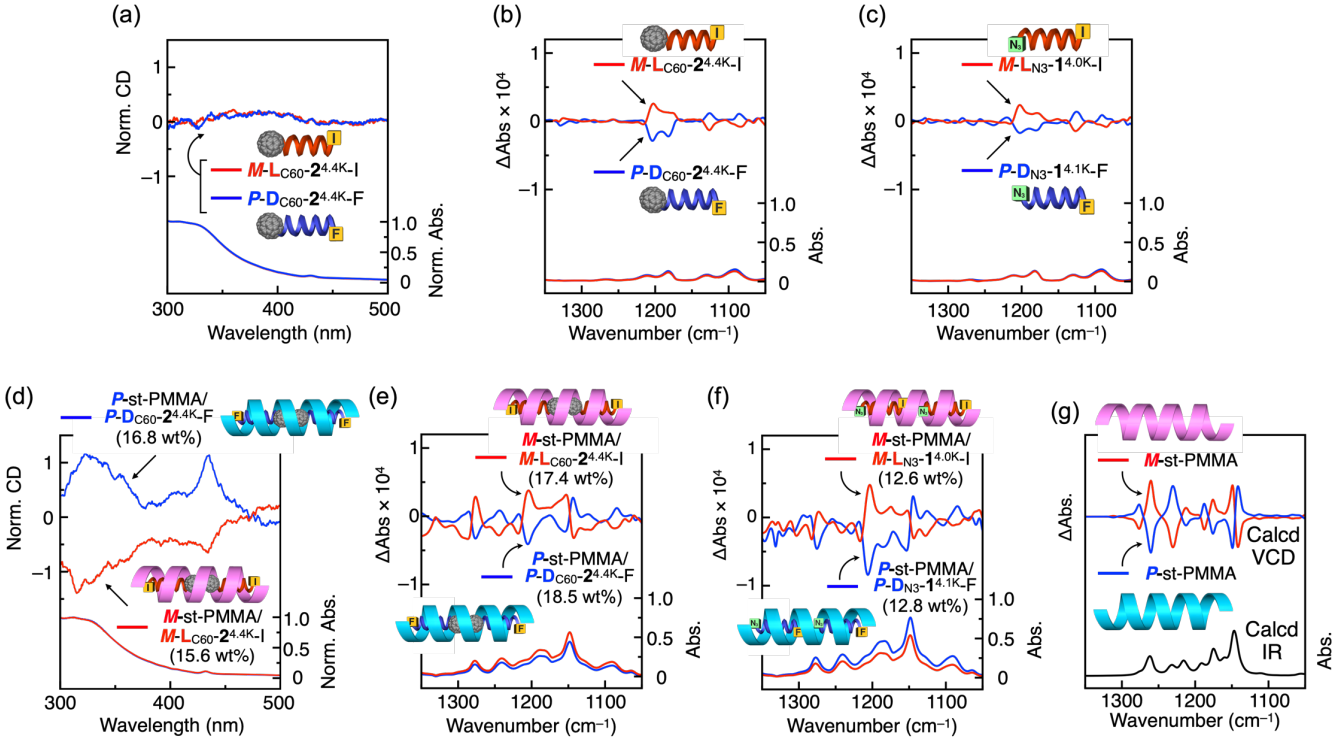

Figure 4. (a,d) ECD (top) and absorption (bottom) spectra of ***M*-L$_{C60}$-2$^{4.4K}$-I** (5.1×10^{-4} M) (red) and ***P*-D$_{C60}$-2$^{4.4K}$-F** (5.3×10^{-4} M) (blue) (a) in toluene-d_8 at 25 °C and those of st-PMMA/***M*-L$_{C60}$-2$^{4.4K}$-I** gel (15.6 wt%) (red) and st-PMMA/***P*-D$_{C60}$-2$^{4.4K}$-F** gel (16.8 wt%) (blue) (d) in toluene at 25 °C. The ECD and absorption spectra in (a,d) were normalized based on the corresponding absorption spectra at 25 °C. The contribution of the linear dichroism caused by the macroscopic anisotropy was negligible (d). The corresponding ECD and absorption spectra of st-PMMA/***M*-L$_{C60}$-2$^{4.4K}$-I** gel containing a higher content of ***M*-L$_{C60}$-2$^{4.4K}$-I** (25.5 wt%) are shown in Figure S11. (b,e) VCD (top) and IR (bottom) spectra of ***M*-L$_{C60}$-2$^{4.4K}$-I** (5.1×10^{-4} M) (red) and ***P*-D$_{C60}$-2$^{4.4K}$-F** (5.3×10^{-4} M) (blue) (b) and those of st-PMMA/***M*-L$_{C60}$-2$^{4.4K}$-I** (17.4 wt%) (red) and st-PMMA/***P*-D$_{C60}$-2$^{4.4K}$-F** (18.5 wt%) (blue) complex gels (e) in toluene-d_8 at room temperature. (c,f) VCD (top) and IR (bottom) spectra of ***M*-L$_{N3}$-1$^{4.0K}$-I** (6.7×10^{-4} M) (red) and ***P*-D$_{N3}$-1$^{4.1K}$-F** (6.7×10^{-4} M) (blue) (c) and those of st-PMMA/***M*-L$_{N3}$-1$^{4.0K}$-I** (12.6 wt%) (red) and st-PMMA/***P*-D$_{N3}$-1$^{4.1K}$-F** (12.8 wt%) (blue) complex gels (f) in toluene-d_8 at room temperature. (g) Calculated VCD (top) and IR (bottom) spectra of *M*- (red line) and *P*- (blue line) helical st-PMMAs.[59]

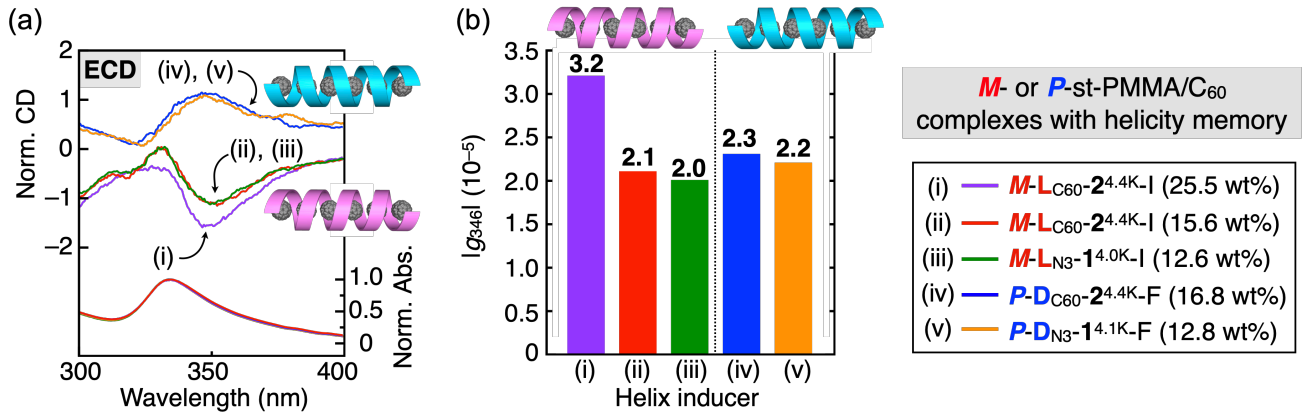

Figure 5. (a) ECD (top) and absorption (bottom) spectra of isolated st-PMMA/C_{60} complex gels in toluene prepared by complexation with ***M*-L**$_{C60}$-**2**$^{4.4K}$-I (i; 25.5 wt%, ii; 15.6 wt%), ***M*-L**$_{N3}$-**1**$^{4.0K}$-I (iii; 12.6 wt%), ***P*-D**$_{C60}$-**2**$^{4.4K}$-F (iv; 16.8 wt%), and ***P*-D**$_{N3}$-**1**$^{4.1K}$-F (v; 12.8 wt%) followed by replacement with the achiral C_{60}. Complete removal of the optically-active PLAs was confirmed by ^{1}H NMR measurements of the isolated st-PMMA/C_{60} complexes (Figure S12). The ECD and absorption spectra were normalized based on the corresponding absorption spectra at 25 °C. (b) Kuhn's dissymmetry factors at 346 nm ($|g_{346}|$) of the isolated st-PMMA/C_{60} complexes (i–v) in (a).

Table 3. Helix-Sense-Selective Encapsulation of C_{60}-Bound Racemic and Nonracemic 2 and C_{60}-Free Racemic 1 by *M*- and *P*-Helical st-PMMA with Helicity Memory [a,b]

run	analyte	handedness of st-PMMA [c]	analyte/ st-PMMA in feed (w/w)	encapsulated analyte		ee (%) of free analyte [f]	separation factor (α) [g]
				yield (%) [d]	ee (%) [e]		
1	*rac*-C_{60}-**2**^{1K}	*M*	0.40	46 (41)	26, *M*-L	19 (18), *P*-D	2.6 (2.4)
2	*rac*-C_{60}-**2**^{1K}	*P*	0.40	47 (42)	22, *P*-D	20 (16), *M*-L	2.3 (2.2)
3	*rac*-C_{60}-**2**^{2K}	*M*	0.37	50 (48)	38, *M*-L	33 (35), *P*-D	4.9 (4.7)
4	*rac*-C_{60}-**2**^{2K}	*P*	0.37	50 (47)	34, *P*-D	34 (31), *M*-L	4.3 (3.8)
5	*rac*-C_{60}-**2**^{4K}	*M*	0.30	52 (55)	49, *M*-L	53 (59), *P*-D	10.4 (11.5)
6	*rac*-C_{60}-**2**^{4K}	*P*	0.30	53 (54)	50, *P*-D	53 (58), *M*-L	10.4 (11.0)
7	*rac*-N_3-**1**^{1K}	*M*	0.23	12	13, *M*-L	2, *P*-D	1.4
8	*rac*-N_3-**1**^{1K}	*P*	0.23	11	13, *P*-D	2, *M*-L	1.4
9	*rac*-N_3-**1**^{2K}	*M*	0.25	23	43, *M*-L	10, *P*-D	3.3
10	*rac*-N_3-**1**^{2K}	*P*	0.25	25	43, *P*-D	13, *M*-L	3.4
11	*rac*-N_3-**1**^{4K}	*M*	0.22	32	61, *M*-L	28, *P*-D	7.3
12	*rac*-N_3-**1**^{4K}	*P*	0.22	32	60, *P*-D	29, *M*-L	7.3
13	53% ee of C_{60}-**2**^{4K} (D-rich)	*M*	0.030	53 (52)	22, *P*-D	87 (87), *P*-D	9.4 (9.2)

[a] Experimental conditions: st-PMMA, 3.0 mg (runs 1–12), 15.0 mg (run 13); (*R*)- or (*S*)-**3**, 75 μL (runs 1–12), (*R*)-**3**, 380 μL (run 13); *rac*-C_{60}-**2**^{1K} (***M*-L**$_{C60}$-**2**$^{1.0K}$-I / ***P*-D**$_{C60}$-**2**$^{1.0K}$-F = 50/50 (mol/mol)), 1.2 mg in 0.50 mL toluene (runs 1,2); *rac*-C_{60}-**2**^{2K} (***M*-L**$_{C60}$-**2**$^{2.4K}$-I / ***P*-D**$_{C60}$-**2**$^{2.5K}$-F = 50/50 (mol/mol)), 1.1 mg in 0.50 mL toluene (runs 3,4); *rac*-C_{60}-**2**^{4K} (***M*-L**$_{C60}$-**2**$^{4.4K}$-I / ***P*-D**$_{C60}$-**2**$^{4.4K}$-F = 50/50 (mol/mol)), 0.89 mg in 0.50 mL toluene (runs 5,6); *rac*-N_3-**1**^{1K} (***M*-L**$_{N3}$-**1**$^{1.0K}$-I / ***P*-D**$_{N3}$-**1**$^{1.0K}$-F = 50/50 (mol/mol)), 0.68 mg in 0.50 mL toluene (runs 7,8); *rac*-N_3-**1**^{2K} (***M*-L**$_{N3}$-**1**$^{2.3K}$-I / ***P*-D**$_{N3}$-**1**$^{2.4K}$-F = 50/50 (mol/mol)), 0.76 mg in 0.50 mL toluene (runs 9,10); *rac*-N_3-**1**^{4K} (***M*-L**$_{N3}$-**1**$^{4.0K}$-I / ***P*-D**$_{N3}$-**1**$^{4.1K}$-F = 50/50 (mol/mol)), 0.67 mg in 0.50 mL toluene (runs 11,12); 53% ee of C_{60}-**2**^{4K} (D-rich) (***M*-L**$_{C60}$-**2**$^{4.4K}$-I / ***P*-D**$_{C60}$-**2**$^{4.4K}$-F = 23/77 (mol/mol)), 0.44 mg in 2.5 mL toluene (run 13). [b] Average values of two runs. [c] *M* and *P* denote left- and right-handed helical senses, respectively. [d] Determined by ^{1}H NMR. In parentheses are shown the values estimated by absorption measurements (runs 1–6 and 13). [e] Determined by ^{1}H NMR. [f] Determined by ^{1}H NMR. In parentheses are shown the calculated ee values based on the yields determined by absorption measurements and the ee values of the encapsulated analytes (runs 1–6 and 13). [g] Calculated according to the equation $\alpha = (F_{major}\ (\%)/F_{minor}\ (\%))/(A_{major}\ (\%)/A_{minor}\ (\%))$, where F_{major} and F_{minor} are the percentages of major and minor enantiomers of the free analyte in the supernatant solutions, respectively, and A_{major} and A_{minor} are those of major and minor enantiomers of the encapsulated analyte, respectively. F_{major}, F_{minor}, A_{major}, and A_{minor} are calculated from the yield and ee of the encapsulated analytes determined by ^{1}H NMR. In parentheses are shown the calculated ee values based on the yields determined by absorption measurements and the ee values of the encapsulated analytes (runs 1–6 and 13). [h] Values of a single experiment.

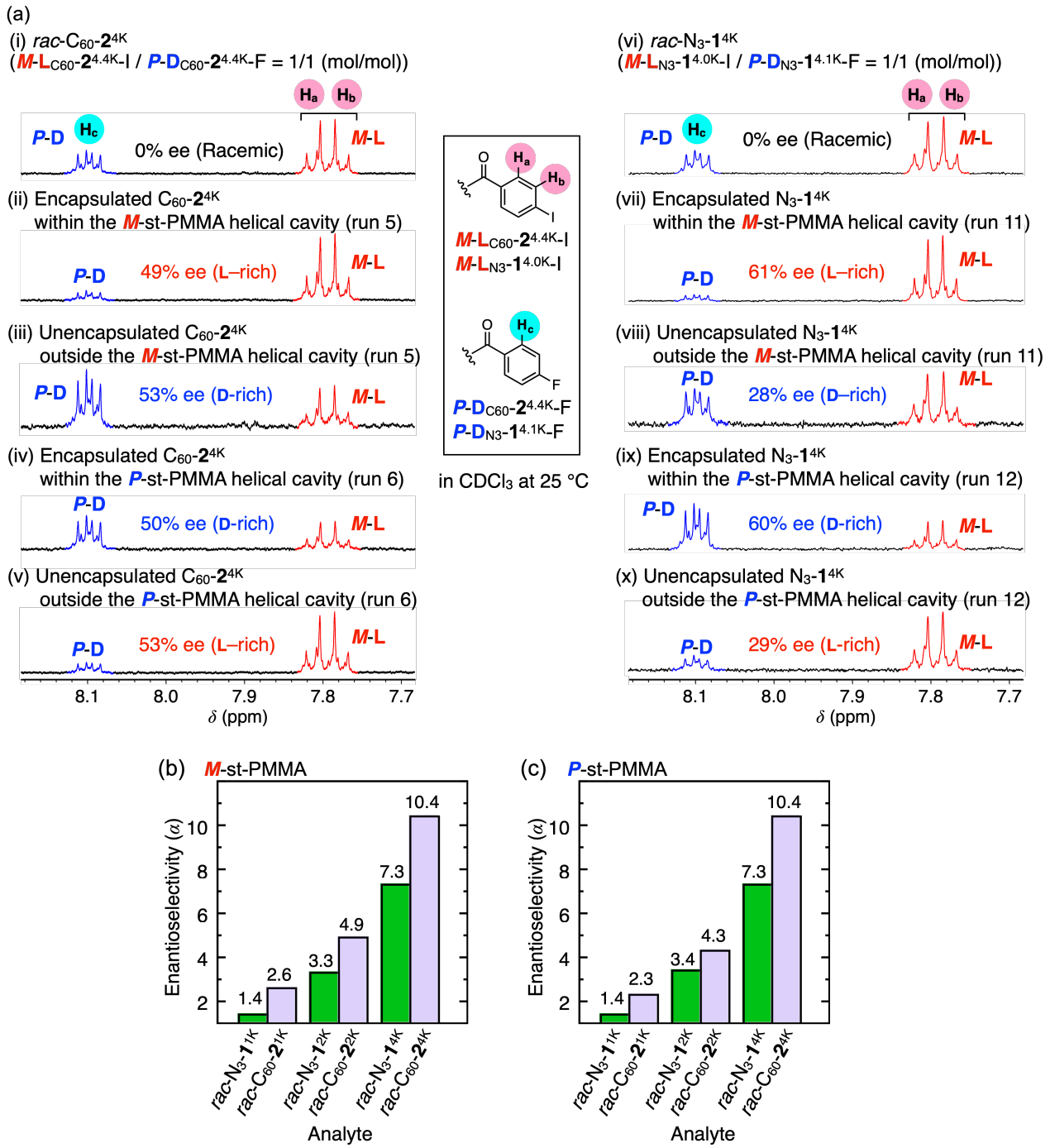

Figure 6. (a) ^{1}H NMR ($CDCl_3$, 25 °C) spectra of *rac*-C_{60}-**2**^{4K} (i) and helix-sense selectively encapsulated C_{60}-**2**^{4K} (L-rich (ii) or D-rich (iv)) and unencapsulated C_{60}-**2**^{4K} (D-rich (iii) or L-rich (v)) in the *M*- (ii and iii) (run 5, Table 3) and *P*- (iv and v) (run 6, Table 3) helical st-PMMA, respectively, and those of *rac*-N_3-**1**^{4K} (vi) and helix-sense selectively encapsulated N_3-**1**^{4K} (L-rich (vii) or D-rich (ix)) and unencapsulated N_3-**1**^{4K} (D-rich (viii) or L-rich (x)) in the *M*- (vii and viii) (run 11, Table 3) and *P*- (ix and x) (run 12, Table 3) helical st-PMMA, respectively. (b,c) Separation factors (enantioselectivity) (α) on *M*-st-PMMA (b) and *P*-st-PMMA (c) for *rac*-N_3-**1** (green bar) and *rac*-C_{60}-**2** (purple bar) with different molar masses. For experimental conditions, see Section 7 in the SI.

Helix-Sense-Selective Encapsulation of C_{60}-Bound and C_{60}-Free PLAs within the Helical Cavity of *M*- and *P*-st-PMMA with a Helicity Memory. Enantioselective extractions of the racemic C_{60}-bound (*rac*-C_{60}-**2**) and C_{60}-free (*rac*-N_3-**1**) *M*- and *P*-PLAs with a different $M_{n,NMR}$ and the end groups by the *M*- and *P*-st-PMMAs with a helicity memory were then performed (Figure 1c). The optically-active *M*- and *P*-st-PMMAs with an excess single-handed helix were prepared according to a previously reported method using (*R*)- and (*S*)-**3** as the chiral solvent by heating at 110 °C, followed by cooling to room temperature, resulting in the gels composed of the *M*- and *P*-st-PMMAs, respectively, which were then repeatedly washed with toluene to completely remove (*R*)- and (*S*)-**3**, then isolated by centrifugation.[61,62]

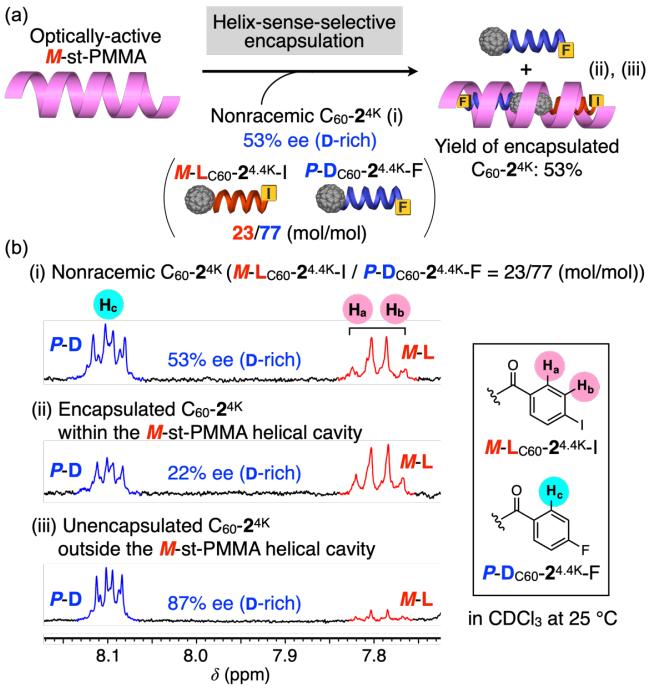

Figure 7. (a) Schematic illustration of the helix-sense-selective encapsulation of the C_{60}-bound nonracemic C_{60}-**2**^{4K} with *M*-st-PMMA with a helicity memory. (b) ^{1}H NMR ($CDCl_3$, 25 °C) spectra of 53% ee of C_{60}-**2**^{4K} (D-rich) (i) and helix-sense selectively encapsulated C_{60}-**2**^{4K} (D-rich; ii) and unencapsulated C_{60}-**2**^{4K} (D-rich; iii) in the *M*-st-PMMA (run 13, Table 3). For experimental conditions, see Section 9 in the SI.

Typically, the condensed *M*-st-PMMA gel (3.0 mg) prepared by (*R*)-**3** was suspended in a toluene solution of *rac*-C_{60}-**2**^{4K} composed of an equal mixture of ***M***-$\mathbf{L}_{C60}$-**2**$^{4.4K}$-I and ***P***-$\mathbf{D}_{C60}$-**2**$^{4.4K}$-F (1.8 mg/mL, 0.50 mL) with stirring at room temperature for 3 h to produce the *M*-st-PMMA/C_{60}-**2**^{4K} complex gel,[96] in which 0.47 mg of the nonracemic C_{60}-**2**^{4K} (52% yield) was encapsulated within the *M*-st-PMMA cavities as estimated by the ^{1}H NMR of the *M*-st-PMMA/C_{60}-**2**^{4K} complex dissolved in $CDCl_3$ (run 5 in Table 3). The yield of the encapsulated C_{60}-**2**^{4K} was almost consistent with that calculated from the difference in the absorption spectra of the racemic C_{60}-**2**^{4K} in toluene before and after the single extraction (Figure S15a).[59,61,75] The ee value of the encapsulated C_{60}-**2**^{4K} was estimated to be 49% (***M***-$\mathbf{L}_{C60}$-**2**$^{4.4K}$-I rich) by the ^{1}H NMR analysis (run 5 in Table 3 and Figure 6a(ii)). When the opposite (*S*)-**3** was used as the chiral solvent during the helix induction in st-PMMA, the resulting opposite *P*-st-PMMA with the helicity memory enantioselectively extracted the opposite enantiomer of C_{60}-**2**^{4K}, giving 50% ee of C_{60}-**2**^{4K} (***P***-$\mathbf{D}_{C60}$-**2**$^{4.4K}$-F rich) in 53% yield (run 6 in Table 3 and Figures 6a(iv) and S14b). We noted that the ee values of the unencapsulated C_{60}-**2**^{4K} remaining in the supernatants were also determined to be 53 (***P***-$\mathbf{D}_{C60}$-**2**$^{4.4K}$-F rich) and 53% (***M***-$\mathbf{L}_{C60}$-**2**$^{4.4K}$-I rich) when the *M*- and *P*-st-PMMA gels were used, respectively (Figure 6a(iii,v)), which were in reasonably consistent agreement with the calculated ee values based on the amounts and ee of the encapsulated C_{60}-**2**^{4K} (runs 5 and 6 in Table 3).

The enantioselective extraction results of a series of *rac*-N_3-**1** and *rac*-C_{60}-**2** samples with a different $M_{n,NMR}$ and the end groups (azido or C_{60} group) are summarized in Table 3. The results revealed that the helical PLA segments of N_3-**1** and C_{60}-**2** that fit the helical cavities of the st-PMMAs with the same helical handedness as those of the PLAs are preferentially entrapped, which well agrees with the facts that the *M*-L-PLAs and *P*-D-PLAs induced the same *M*- and *P*-helical conformations in the st-PMMA backbone independent of the terminal residues (azido or C_{60} group), respectively, once encapsulated as previously described. The ee values of C_{60}-free **1** and C_{60}-bound **2** enantio- and helix-sense selectively entrapped in the optically-active *M*- and *P*-st-PMMA are variable depending on the amounts (yields) of the encapsulated N_3-**1** and C_{60}-**2**, therefore, we employed the separation factor (enantioselectivity) (α)[97-99] to evaluate the chiral recognition ability of the *M*- and *P*-st-PMMA toward the *rac*-N_3-**1** and *rac*-C_{60}-**2** (Table 3).

The C_{60}-bound PLAs (*rac*-C_{60}-**2**) were more efficiently and enantioselectively encapsulated in the helical cavity of the st-PMMA than the corresponding C_{60}-free *rac*-N_3-**1** under the similar experimental conditions using almost the identical $M_{n,NMR}$ of PLAs, probably because the terminal achiral C_{60} residues of the C_{60}-bound PLAs most likely contribute to enhancing the inclusion complexations with the st-PMMA, which could further enhance the hydrophobic interactions between the chiral PLA chains and the helical cavity of the st-PMMA, resulting in greater encapsulation yields and hence higher α values over the corresponding C_{60}-free PLAs. The enantioselectivity (α value) was highly dependent on the $M_{n,NMR}$ of the C_{60}-free and C_{60}-bound PLAs, and showed a clear tendency that the α value significantly increased with the increasing $M_{n,NMR}$ of the PLAs such that 1.4 < 3.3–3.4 < 7.3 and 2.3–2.6 < 4.3–4.9 < 10.4 for the C_{60}-free *rac*-N_3-**1** and C_{60}-bound *rac*-C_{60}-**2**, respectively (Figure 6b,c and Table 3) and eventually reached the excellent α value of ca. 10, thus giving approximately 50% ee for both the optically-active ***M***- and ***P***-C_{60}-**2**$^{4.4K}$ that could be isolated by a single extraction using *M*- and *P*-st-PMMA, when *rac*-C_{60}-**2** composed of an equal mixture of the highest molar mass PLAs, ***M***-$\mathbf{L}_{C60}$-**2**$^{4.4K}$-I and ***P***-$\mathbf{D}_{C60}$-**2**$^{4.4K}$-F, was used (runs 5 and 6 in Table 3). The observed molar mass-dependent enhancement of the enantioselectivity is most likely due to the effective increases in the one-handed helical chain lengths of the *M*- and *P*-PLAs that allow further enhancement of the hydrophobic chiral interactions with the one-handed st-PMMA helical cavity. Furthermore, when the enantioselective extraction by *M*-st-PMMA with a helicity memory was further performed using nonracemic C_{60}-**2**^{4K} (53% ee (D-rich)) as an analyte that can be obtained by single extraction with *M*-st-PMMA (run 5 in Table 3), the ee value of the unencapsulated C_{60}-**2**^{4K} remaining in the supernatants increased to 87% ee (D-rich) (Figure 7 and run 13 in Table 3), thus providing a practically useful resolution method to obtain both helices of the PLAs with a high optical purity only by two extractions using *M*- or *P*-st-PMMA with a helicity memory.

CONCLUSION

In summary, we have found that the homochiral *M*-L- and *P*-D-PLAs are efficiently encapsulated in a highly helix-sense-selective manner within the helical cavity of an optically-active st-PMMA with memory of the macromolecular helicity, which is readily prepared from inexpensive st-PMMA using chiral amines based on the "helicity induction and memory" strategy, thus producing unique crystalline "helix-in-helix" superstructured inclusion complexes with the same helical

sense to each other. Contrary to the previously observed inclusion complex of st-PMMA with the C_{60}-bound *M*- and *P*-helical peptides,[75] the introduction of a C_{60} moiety at one end of the PLA chains is not necessarily required for the encapsulation in the st-PMMA hollow space, although the C_{60} unit as well as the longer helical chains of the *M*- and *P*-PLAs contributes to significant enhancement of the enantioselectivities during the "helix-in-helix" inclusion complex formations. The present results imply that other varieties of helical as well as nonhelical oligomers and polymers may form similar "helix-in-helix" superstructured inclusion complexes with a controlled handedness once encapsulated within the one-handed helical cavity of the st-PMMA. It should be emphasized that the observed α values of more than 2 (Table 3) are, in general, high enough for the complete base-line separation of enantiomers when used as a CSP for chiral HPLC,[98,99] indicating that the optically-active st-PMMA with an excess one-handedness has the potential as a practically useful CSP for separating not only racemic PLAs, but also other racemic helical oligomers and polymers as well as chiral fullerenes[61] and aromatic compounds,[100] since st-PMMA has successfully been chemically bonded to silica particles by the surface-initiated living syndiotactic-specific anionic polymerization of MMA.[63] Such an immobilized st-PMMA-based CSP has a great advantage such that either an *M*- or *P*-helical st-PMMA can be induced using (*R*)- or (*S*)-**3** and subsequently memorized, thus providing a switchable CSP,[101,102] in which the elution order of chiral analytes can be switched in a reversible fashion. The work to this goal is now in progress in our group.

ASSOCIATED CONTENT

Supporting Information

The Supporting Information is available free of charge on the ACS Publications website at DOI: XXX

Full experimental details, characterizations of C_{60}-free and C_{60}-bound *M*- and *P*-PLAs and their inclusion complexes with st-PMMA, and additional supporting data (PDF).

AUTHOR INFORMATION

Corresponding Author

*yashima@chembio.nagoya-u.ac.jp

ORCID

Tomoyuki Ikai: 0000-0002-5211-2421
Daisuke Taura: 0000-0002-5396-5573
Naoki Ousaka: 0000-0002-3398-3328
Eiji Yashima: 0000-0001-6307-198X

Present Addresses

§N.O.: Molecular Engineering Institute, Kyushu Institute of Technology, Tobata-ku, Kitakyushu, 804-8550, Japan.

Notes

The authors declare no competing financial interest.

ACKNOWLEDGMENT

This work was supported in part by JSPS KAKENHI (Grant-in-Aid for Specially Promoted Research, no. 18H05209 (E.Y. and T.I.)). The authors thank Prof. Rong-Ming Ho (National Tsing Hua University, Taiwan) for his kind supply of D-lactide.

REFERENCES

(1) Bishop, R.; Dance, I. G. New Types of Helical Canal Inclusion Networks. *Top. Curr. Chem.* **1988**, *149*, 137–188.

(2) Star, A.; Steuerman, D. W.; Heath, J. R.; Stoddart, J. F. Starched Carbon Nanotubes. *Angew. Chem., Int. Ed.* **2002**, *41*, 2508–2512.

(3) Kim, O.-K.; Je, J.; Baldwin, J. W.; Kooi, S.; Pehrsson, P. E.; Buckley, L. J. Solubilization of Single-Wall Carbon Nanotubes by Supramolecular Encapsulation of Helical Amylose. *J. Am. Chem. Soc.* **2003**, *125*, 4426–4427.

(4) Li, C.; Numata, M.; Bae, A.-H.; Sakurai, K.; Shinkai, S. Self-Assembly of Supramolecular Chiral Insulated Molecular Wire. *J. Am. Chem. Soc.* **2005**, *127*, 4548–4549.

(5) Sanji, T.; Kato, N.; Kato, M.; Tanaka, M. Helical Folding in a Helical Channel: Chiroptical Transcription of Helical Information through Chiral Wrapping. *Angew. Chem., Int. Ed.* **2005**, *44*, 7301–7304.

(6) Ikeda, M.; Furusho, Y.; Okoshi, K.; Tanahara, S.; Maeda, K.; Nishino, S.; Mori, T.; Yashima, E. A Luminescent Poly(phenylenevinylene)–Amylose Composite with Supramolecular Liquid Crystallinity. *Angew. Chem., Int. Ed.* **2006**, *45*, 6491–6495.

(7) Sanji, T.; Kato, N.; Tanaka, M. Chirality Control in Oligothiophene through Chiral Wrapping. *Org. Lett.* **2006**, *8*, 235–238.

(8) Frampton, M. J.; Claridge, T. D. W.; Latini, G.; Brovelli, S.; Cacialli, F.; Anderson, H. L. Amylose-Wrapped Luminescent Conjugated Polymers. *Chem. Commun.* **2008**, 2797–2799.

(9) Numata, M.; Shinkai, S. 'Supramolecular Wrapping Chemistry' by Helix-Forming Polysaccharides: A Powerful Strategy for Generating Diverse Polymeric Nano-Architectures. *Chem. Commun.* **2011**, *47*, 1961–1975.

(10) Kumar, K.; Woortman, A. J. J.; Loos, K. Synthesis of Amylose–Polystyrene Inclusion Complexes by a Facile Preparation Route. *Biomacromolecules* **2013**, *14*, 1955–1960.

(11) Klug, A. From Macromolecules to Biological Assemblies (Nobel Lecture). *Angew. Chem., Int. Ed. Engl.* **1983**, *22*, 565–582.

(12) Egan, P.; Sinko, R.; LeDuc, P. R.; Keten, S. The Role of Mechanics in Biological and Bio-Inspired Systems. *Nat. Commun.* **2015**, *6*, 7418.

(13) Luo, Q.; Hou, C.; Bai, Y.; Wang, R.; Liu, J. Protein Assembly: Versatile Approaches to Construct Highly Ordered Nanostructures. *Chem. Rev.* **2016**, *116*, 13571–13632.

(14) Pieters, B. J. G. E.; van Eldijk, M. B.; Nolte, R. J. M.; Mecinović, J. Natural Supramolecular Protein Assemblies. *Chem. Soc. Rev.* **2016**, *45*, 24–39.

(15) Wilson, C. J.; Bommarius, A. S.; Champion, J. A.; Chernoff, Y. O.; Lynn, D. G.; Paravastu, A. K.; Liang, C.; Hsieh, M.-C.; Heemstra, J. M. Biomolecular Assemblies: Moving from Observation to Predictive Design. *Chem. Rev.* **2018**, *118*, 11519–11574.

(16) Yuan, C.; Ji, W.; Xing, R.; Li, J.; Gazit, E.; Yan, X. Hierarchically Oriented Organization in Supramolecular Peptide Crystals. *Nat. Rev. Chem.* **2019**, *3*, 567–588.

(17) Tomasik, P.; Schilling, C. H. Complexes of Starch with Organic Guests. *Adv. Carbohydr. Chem. Biochem.* **1998**, *53*, 345–426.

(18) Frampton, M. J.; Anderson, H. L. Insulated Molecular Wires. *Angew. Chem., Int. Ed.* **2007**, *46*, 1028–1064.

(19) Putseys, J. A.; Lamberts, L.; Delcour, J. A. Amylose-Inclusion Complexes: Formation, Identity and Physico-Chemical Properties. *J. Cereal Sci.* **2010**, *51*, 238–247.

(20) Alberts, B.; Johnson, A.; Lewis, J.; Morgan, D.; Raff, M.; Roberts, K.; Walter, P.*; Molecular biology of the cell, 6th ed., Garland Science*: New York, 2015.

(21) Kadokawa, J. Synthesis of Amylosic Supramolecular Materials by Glucan Phosphorylase-Catalyzed Enzymatic Polymerization According to the Vine-Twining Approach. *Synlett* **2020**, *31*, 648–656.

(22) Barrow, S. J.; Kasera, S.; Rowland, M. J.; del Barrio, J.; Scherman, O. A. Cucurbituril-Based Molecular Recognition. *Chem. Rev.* **2015**, *115*, 12320–12406.

(23) Li, J.; Yim, D.; Jang, W.-D.; Yoon, J. Recent Progress in the Design and Applications of Fluorescence Probes Containing Crown Ethers. *Chem. Soc. Rev.* **2017**, *46*, 2437–2458.

(24) Liu, Z.; Nalluri, S. K. M.; Stoddart, J. F. Surveying Macrocyclic Chemistry: From Flexible Crown Ethers to Rigid Cyclophanes. *Chem. Soc. Rev.* **2017**, *46*, 2459–2478.

(25) Murray, J.; Kim, K.; Ogoshi, T.; Yao, W.; Gibb, B. C. The Aqueous Supramolecular Chemistry of Cucurbit[*n*]urils, Pillar[*n*]arenes and Deep-Cavity Cavitands. *Chem. Soc. Rev.* **2017**, *46*, 2479–2496.

(26) Prochowicz, D.; Kornowicz, A.; Lewiński, J. Interactions of Native Cyclodextrins with Metal Ions and Inorganic Nanoparticles: Fertile Landscape for Chemistry and Materials Science. *Chem. Rev.* **2017**, *117*, 13461–13501.

(27) Kumar, R.; Sharma, A.; Singh, H.; Suating, P.; Kim, H. S.; Sunwoo, K.; Shim, I.; Gibb, B. C.; Kim, J. S. Revisiting Fluorescent Calixarenes: From Molecular Sensors to Smart Materials. *Chem. Rev.* **2019**, *119*, 9657–9721.

(28) Ogoshi, T.; Kakuta, T.; Yamagishi, T. Applications of Pillar[*n*]arene-Based Supramolecular Assemblies. *Angew. Chem., Int. Ed.* **2019**, *58*, 2197–2206.

(29) Blanco-Gómez, A.; Cortón, P.; Barravecchia, L.; Neira, I.; Pazos, E.; Peinador, C.; García, M. D. Controlled Binding of Organic Guests by Stimuli-Responsive Macrocycles. *Chem. Soc. Rev.* **2020**, *49*, 3834–3862.

(30) Xia, D.; Wang, P.; Ji, X.; Khashab, N. M.; Sessler, J. L.; Huang, F. Functional Supramolecular Polymeric Networks: The Marriage of Covalent Polymers and Macrocycle-Based Host–Guest Interactions. *Chem. Rev.* **2020**, *120*, 6070–6123.

(31) Biros, S. M.; Rebek, J. J. Structure and Binding Properties of Water-Soluble Cavitands and Capsules. *Chem. Soc. Rev.* **2007**, *36*, 93–104.

(32) Saalfrank, R. W.; Maid, H.; Scheurer, A. Supramolecular Coordination Chemistry: The Synergistic Effect of Serendipity and Rational Design. *Angew. Chem., Int. Ed.* **2008**, *47*, 8794–8824.

(33) Yoshizawa, M.; Klosterman, J. K.; Fujita, M. Functional Molecular Flasks: New Properties and Reactions within Discrete, Self-Assembled Hosts. *Angew. Chem., Int. Ed.* **2009**, *48*, 3418–3438.

(34) Brown, C. J.; Toste, F. D.; Bergman, R. G.; Raymond, K. N. Supramolecular Catalysis in Metal–Ligand Cluster Hosts. *Chem. Rev.* **2015**, *115*, 3012–3035.

(35) Rizzuto, F. J.; von Krbek, L. K. S.; Nitschke, J. R. Strategies for Binding Multiple Guests in Metal–Organic Cages. *Nat. Rev. Chem.* **2019**, *3*, 204–222.

(36) Yoshizawa, M.; Catti, L. Bent Anthracene Dimers as Versatile Building Blocks for Supramolecular Capsules. *Acc. Chem. Res.* **2019**, *52*, 2392–2404.

(37) Pilgrim, B. S.; Champness, N. R. Metal-Organic Frameworks and Metal-Organic Cages – A Perspective. *ChemPlusChem* **2020**, *85*, 1842–1856.

(38) Sun, Y.; Chen, C.; Liu, J.; Stang, P. J. Recent Developments in the Construction and Applications of Platinum-Based Metallacycles and Metallacages via Coordination. *Chem. Soc. Rev.* **2020**, *49*, 3889–3919.

(39) Hill, D. J.; Mio, M. J.; Prince, R. B.; Hughes, T. S.; Moore, J. S. A Field Guide to Foldamers. *Chem. Rev.* **2001**, *101*, 3893–4011.

(40) Ho, R.-M.; Chiang, Y.-W.; Lin, S.-C.; Chen, C.-K. Helical Architectures from Self-Assembly of Chiral Polymers and Block Copolymers. *Prog. Polym. Sci.* **2011**, *36*, 376–453.

(41) Pfukwa, R.; Kouwer, P. H. J.; Rowan, A. E.; Klumperman, B. Templated Hierarchical Self-Assembly of Poly(*p*-aryltriazole) Foldamers. *Angew. Chem., Int. Ed.* **2013**, *52*, 11040–11044.

(42) Yashima, E.; Ousaka, N.; Taura, D.; Shimomura, K.; Ikai, T.; Maeda, K. Supramolecular Helical Systems: Helical Assemblies of Small Molecules, Foldamers, and Polymers with Chiral Amplification and Their Functions. *Chem. Rev.* **2016**, *116*, 13752–13990.

(43) Ferrand, Y.; Huc, I. Designing Helical Molecular Capsules Based on Folded Aromatic Amide Oligomers. *Acc. Chem. Res.* **2018**, *51*, 970–977.

(44) John, E. A.; Massena, C. J.; Berryman, O. B. Helical Anion Foldamers in Solution. *Chem. Rev.* **2020**, *120*, 2759–2782.

(45) Legrand, B.; Aguesseau-Kondrotas, J.; Simon, M.; Maillard, L. Catalytic Foldamers: When the Structure Guides the Function. *Catalysts* **2020**, *10*.

(46) Rinaldi, S. The Diverse World of Foldamers: Endless Possibilities of Self-Assembly. *Molecules* **2020**, *25*.

(47) Tamura, K.; Sam, N. S. M.; Ikai, T.; Okamoto, Y.; Yashima, E. Synthesis and Chiral Recognition Ability of a Poly(phenylenevinylene)-Encapsulated Amylose Derivative. *Bull. Chem. Soc. Jpn.* **2011**, *84*, 741–747.

(48) Zheng, M.; Jagota, A.; Semke, E. D.; Diner, B. A.; McLean, R. S.; Lustig, S. R.; Richardson, R. E.; Tassi, N. G. DNA-Assisted Dispersion and Separation of Carbon Nanotubes. *Nat. Mater.* **2003**, *2*, 338–342.

(49) Sakurai, K.; Uezu, K.; Numata, M.; Hasegawa, T.; Li, C.; Kaneko, K.; Shinkai, S. β-1,3-Glucan Polysaccharides as Novel One-Dimensional Hosts for DNA/RNA, Conjugated Polymers and Nanoparticles. *Chem. Commun.* **2005**, 4383–4398.

(50) Nishino, S.; Mori, T.; Tanahara, S.; Maeda, K.; Ikeda, M.; Furusho, Y.; Yashima, E. Application of Soluble Poly(phenylenevinylene) Wrapped in Amylose to Organic Light-Emitting Diodes. *Mol. Cryst. Liq. Cryst.* **2007**, *471*, 29–38.

(51) Akazaki, K.; Toshimitsu, F.; Ozawa, H.; Fujigaya, T.; Nakashima, N. Recognition and One-Pot Extraction of Right- and Left-Handed Semiconducting Single-Walled Carbon Nanotube Enantiomers Using Fluorene-Binaphthol Chiral Copolymers. *J. Am. Chem. Soc.* **2012**, *134*, 12700–12007.

(52) Chung, W.; Nobusawa, K.; Kamikubo, H.; Kataoka, M.; Fujiki, M.; Naito, M. Time-Resolved Observation of Chiral-Index-Selective Wrapping on Single-Walled Carbon Nanotube with Non-Aromatic Polysilane. *J. Am. Chem. Soc.* **2013**, *135*, 2374–2383.

(53) Deria, P.; Von Bargen, C. D.; Olivier, J.-H.; Kumbhar, A. S.; Saven, J. G.; Therien, M. J. Single-Handed Helical Wrapping of Single-Walled Carbon Nanotubes by Chiral, Ionic, Semiconducting Polymers. *J. Am. Chem. Soc.* **2013**, *135*, 16220–16234.

(54) Sun, J. Z.; Qin, A.; Tang, B. Z. Functional Polyacetylenes: Hybrids with Carbon Nanotubes. *Polym. Chem.* **2013**, *4*, 211–223.

(55) Schroeder, V.; Savagatrup, S.; He, M.; Lin, S.; Swager, T. M. Carbon Nanotube Chemical Sensors. *Chem. Rev.* **2019**, *119*, 599–663.

(56) Haraguchi, S.; Numata, M.; Li, C.; Nakano, Y.; Fujiki, M.; Shinkai, S. Circularly Polarized Luminescence from Supramolecular Chiral Complexes of Achiral Conjugated Polymers and a Neutral Polysaccharide. *Chem. Lett.* **2009**, *38*, 254–255.

(57) Shiraki, T.; Tsuchiya, Y.; Noguchi, T.; Tamaru, S.; Suzuki, N.; Taguchi, M.; Fujiki, M.; Shinkai, S. Creation of Circularly Polarized Luminescence from an Achiral Polyfluorene Derivative through Complexation with Helix-Forming Polysaccharides: Importance of the *meta*-Linkage Chain for Helix Formation. *Chem. - Asian J.* **2014**, *9*, 218–222.

(58) Peters, K. Polymer Optical Fiber Sensors–A Review. *Smart Mater. Struct.* **2011**, *20*, 013002.

(59) Kawauchi, T.; Kumaki, J.; Kitaura, A.; Okoshi, K.; Kusanagi, H.; Kobayashi, K.; Sugai, T.; Shinohara, H.; Yashima, E. Encapsulation of Fullerenes in a Helical PMMA Cavity Leading to a Robust Processable Complex with a Macromolecular Helicity Memory. *Angew. Chem., Int. Ed.* **2008**, *47*, 515–519.

(60) Kawauchi, T.; Kitaura, A.; Kumaki, J.; Kusanagi, H.; Yashima, E. Helix-Sense-Controlled Synthesis of Optically Active Poly(methyl methacrylate) Stereocomplexes. *J. Am. Chem. Soc.* **2008**, *130*, 11889–11891.

(61) Kawauchi, T.; Kitaura, A.; Kawauchi, M.; Takeichi, T.; Kumaki, J.; Iida, H.; Yashima, E. Separation of C_{70} over C_{60} and Selective Extraction and Resolution of Higher Fullerenes by Syndiotactic Helical Poly(methyl methacrylate). *J. Am. Chem. Soc.* **2010**, *132*, 12191–12193.

(62) Kitaura, A.; Iida, H.; Kawauchi, T.; Yashima, E. Helicity Induction and Memory of Syndiotactic Poly(methyl methacrylate) Assisted by Optically Active Additives and Solvents and Chiral Amplification of Helicity. *Chem. Lett.* **2011**, *40*, 28–30.

(63) Sato, M.; Kato, T.; Ohishi, T.; Ishige, R.; Ohta, N.; White, K. L.; Hirai, T.; Takahara, A. Precise Synthesis of Poly(methyl methacrylate) Brush with Well-Controlled Stereoregularity Using a Surface-Initiated Living Anionic Polymerization Method. *Macromolecules* **2016**, *49*, 2071–2076.

(64) Vidal, F.; Falivene, L.; Caporaso, L.; Cavallo, L.; Chen, E. Y. X. Robust Cross-Linked Stereocomplexes and C_{60} Inclusion Complexes of Vinyl-Functionalized Stereoregular Polymers Derived from Chemo/Stereoselective Coordination Polymerization. *J. Am. Chem. Soc.* **2016**, *138*, 9533–9547.

(65) Sato, M.; Kato, T.; Shimamoto, H.; Kamitani, K.; Ohta, N.; Hirai, T.; Takahara, A. Design of High-Density Helical Polymer Brush on Silica Nanoparticles for the Size Recognition of Fullerene Molecules. *ACS Macro Lett.* **2018**, *7*, 148–152.

(66) Kumaki, J.; Kawauchi, T.; Okoshi, K.; Kusanagi, H.; Yashima, E. Supramolecular Helical Structure of the Stereocomplex Composed of Complementary Isotactic and Syndiotactic Poly(methyl methacrylate)s as Revealed by Atomic Force Microscopy. *Angew. Chem., Int. Ed.* **2007**, *46*, 5348–5351.

(67) Stereocomplex formation has been applied to construct supramolecular nanostructures, see refs. 68–74.

(68) Kawauchi, T.; Kumaki, J.; Yashima, E. Nanosphere and Nanonetwork Formations of [60]Fullerene-End-Capped Stereoregular Poly(methyl methacrylate)s through Stereocomplex Formation Combined with Self-Assembly of the Fullerenes. *J. Am. Chem. Soc.* **2006**, *128*, 10560–10567.

(69) Goh, T. K.; Tan, J. F.; Guntari, S. N.; Satoh, K.; Blencowe, A.; Kamigaito, M.; Qiao, G. G. Nano-to-Macroscale Poly(methyl methacrylate) Stereocomplex Assemblies. *Angew. Chem., Int. Ed.* **2009**, *48*, 8707–8711.

(70) Ren, J. M.; Ishitake, K.; Satoh, K.; Blencowe, A.; Fu, Q.; Wong, E. H. H.; Kamigaito, M.; Qiao, G. G. Stereoregular High-Density Bottlebrush Polymer and Its Organic Nanocrystal Stereocomplex through Triple-Helix Formation. *Macromolecules* **2016**, *49*, 788–795.

(71) Ren, J. M.; Lawrence, J.; Knight, A. S.; Abdilla, A.; Zerdan, R. B.; Levi, A. E.; Oschmann, B.; Gutekunst, W. R.; Lee, S.-H.; Li, Y.; McGrath, A. J.; Bates, C. M.; Qiao, G. G.; Hawker, C. J. Controlled Formation and Binding Selectivity of Discrete Oligo(methyl methacrylate) Stereocomplexes. *J. Am. Chem. Soc.* **2018**, *140*, 1945–1951.

(72) Ren, J. M.; Knight, A. S.; van Ravensteijn, B. G. P.; Kohl, P.; Bou Zerdan, R.; Li, Y.; Lunn, D. J.; Abdilla, A.; Qiao, G. G.; Hawker, C. J. DNA-Inspired Strand-Exchange for Switchable PMMA-Based Supramolecular Morphologies. *J. Am. Chem. Soc.* **2019**, *141*, 2630–2635.

(73) Vidal, F.; Watson, E. M.; Chen, E. Y. X. All-Methacrylic Stereoregular Triblock Co-polymer Thermoplastic Elastomers Toughened by Supramolecular Stereocomplexation. *Macromolecules* **2019**, *52*, 7313–7323.

(74) Abdilla, A.; Dolinski, N. D.; de Roos, P.; Ren, J. M.; van der Woude, E.; Seo, S. E.; Zayas, M. S.; Lawrence, J.; Read de Alaniz, J.; Hawker, C. J. Polymer Stereocomplexation as a Scalable Platform for Nanoparticle Assembly. *J. Am. Chem. Soc.* **2020**, *142*, 1667–1672.

(75) Ousaka, N.; Mamiya, F.; Iwata, Y.; Nishimura, K.; Yashima, E. "Helix-in-Helix" Superstructure Formation through Encapsulation of Fullerene-Bound Helical Peptides within a Helical Poly(methyl methacrylate) Cavity. *Angew. Chem., Int. Ed.* **2017**, *56*, 791–795.

(76) Kawauchi, T.; Ohnishi, K.; Kajihara, K.; Kawauchi, M.; Takeichi, T. Polymer Alloying of Helical Syndiotactic PMMA with [60]Fullerene-End-Capped Polymers through Inclusion Complex Formation of the Helical Cavity with Fullerene Units. *Macromolecules* **2019**, *52*, 5067–5073.

(77) *Poly(Lactic Acid): Synthesis, Structures, Properties, Processing, and Applications*; Auras, R., Lim, L. T., Selke, S. E. M., Tsuji, H., Eds.; John Wiley & Sons. Inc.: NJ, 2010.

(78) De Santis, P.; Kovacs, A. J. Molecular Conformation of Poly(S-lactic Acid). **1968**, *6*, 299–306.

(79) Sasaki, S.; Asakura, T. Helix Distortion and Crystal Structure of the α-Form of Poly(L-lactide). *Macromolecules* **2003**, *36*, 8385–8390.

(80) Wasanasuk, K.; Tashiro, K.; Hanesaka, M.; Ohhara, T.; Kurihara, K.; Kuroki, R.; Tamada, T.; Ozeki, T.; Kanamoto, T. Crystal Structure Analysis of Poly(L-lactic Acid) α Form On the basis of the 2-Dimensional Wide-Angle Synchrotron X-ray and Neutron Diffraction Measurements. *Macromolecules* **2011**, *44*, 6441–6452.

(81) Tonelli, A. E. Polylactides in Channels. *Macromolecules* **1992**, *25*, 3581–3584.

(82) Topol, I. A.; Burt, S. K.; Deretey, E.; Tang, T.-H.; Perczel, A.; Rashin, A.; Csizmadia, I. G. α- and 3_{10}-Helix Interconversion: A Quantum-Chemical Study on Polyalanine Systems in the Gas Phase and in Aqueous Solvent. *J. Am. Chem. Soc.* **2001**, *123*, 6054–6060.

(83) Nolte, R. J. M.; Van Beijnen, A. J. M.; Drenth, W. Chirality in Polyisocyanides. *J. Am. Chem. Soc.* **1974**, *96*, 5932–5933.

(84) Okamoto, Y.; Mohri, H.; Nakano, T.; Hatada, K. Stereomutation of Optically Active Poly(diphenyl-2-pyridylmethyl methacrylate). *J. Am. Chem. Soc.* **1989**, *111*, 5952–5954.

(85) Miyabe, T.; Iida, H.; Banno, M.; Yamaguchi, T.; Yashima, E. Synthesis and Visualization of a Core Cross-Linked Star Polymer Carrying Optically Active Rigid-Rod Helical Polyisocyanide Arms and Its Chiral Recognition Ability. *Macromolecules* **2011**, *44*, 8687–8692.

(86) Ohya, Y.; Takamido, S.; Nagahama, K.; Ouchi, T.; Ooya, T.; Katoono, R.; Yui, N. Molecular "Screw and Nut": *α*-Cyclodextrin Recognizes Polylactide Chirality. *Macromolecules* **2007**, *40*, 6441–6444.

(87) Kaneko, Y.; Ueno, K.; Yui, T.; Nakahara, K.; Kadokawa, J.-i. Amylose's Recognition of Chirality in Polylactides on Formation of Inclusion Complexes in Vine-Twining Polymerization. *Macromol. Biosci.* **2011**, *11*, 1407–1415.

(88) Tanaka, T.; Sasayama, S.; Yamamoto, K.; Kimura, Y.; Kadokawa, J.-i. Evaluating Relative Chain Orientation of Amylose and Poly(L-lactide) in Inclusion Complexes Formed by Vine-Twining Polymerization Using Primer-Guest Conjugates. *Macromol. Chem. Phys.* **2015**, *216*, 794–800.

(89) Isono, T.; Kondo, Y.; Otsuka, I.; Nishiyama, Y.; Borsali, R.; Kakuchi, T.; Satoh, T. Synthesis and Stereocomplex Formation of Star-Shaped Stereoblock Polylactides Consisting of Poly(L-lactide) and Poly(D-lactide) Arms. *Macromolecules* **2013**, *46*, 8509‑8518.

(90) Abe, H.; Imai, K.; Matsumoto, M. Syndiotactic Polymerization of Methyl Methacrylate. *J. Polym. Sci., Part C* **1968**, *23*, 469–485.

(91) Fox, T. G.; Garrett, B. S.; Goode, W. E.; Gratch, S.; Kincaid, J. F.; Spell, A.; Stroupe, J. D. Crystalline Polymers of Methyl Methacrylate. *J. Am. Chem. Soc.* **1958**, *80*, 1768–1769.

(92) Liquori, A. M.; Anzuino, G.; Coiro, V. M.; D'Alagni, M.; De Santis, P.; Savino, M. Complementary Stereospecific Interaction Between Isotactic and Syndiotactic Polymer Molecules. *Nature* **1965**, *206*, 358–362.

(93) Worch, J. C.; Prydderch, H.; Jimaja, S.; Bexis, P.; Becker, M. L.; Dove, A. P. Stereochemical Enhancement of Polymer Properties. *Nat. Rev. Chem.* **2019**, *3*, 514–535.

(94) Effing, J.; Jonas, U.; Jullien, L.; Plesnivy, T.; Ringsdorf, H.; Diederich, F.; Thilgen, C.; Weinstein, D. C_{60} and C_{70} in a Basket? – Investigations of Mono- and Multilayers from Azacrown Compounds and Fullerenes. *Angew. Chem., Int. Ed. Engl.* **1992**, *31*, 1599–1602.

(95) Pantoş, G. D.; Wietor, J.-L.; Sanders, J. K. M. Filling Helical Nanotubes with C_{60}. *Angew. Chem., Int. Ed.* **2007**, *46*, 2238–2240.

(96) The PLA chain exchange reactions between the C_{60}-bound helical ***M***- or ***P***-PLAs encapsulated in the *M*-st-PMMA helical cavity and free C_{60}-bound helical ***M***- or ***P***-PLAs proceeded to reach an equilibrium within 3 h at room temperature (see Figure S14 and Section 8 in the SI).

(97) The *α* value is a useful measure in chiral chromatography to evaluate the chiral resolving abilities of CSPs toward racemic analytes, see refs. 97 and 98.

(98) Okamoto, Y.; Yashima, E. Polysaccharide Derivatives for Chromatographic Separation of Enantiomers. *Angew. Chem., Int. Ed.* **1998**, *37*, 1020–1043.

(99) Shen, J.; Okamoto, Y. Efficient Separation of Enantiomers Using Stereoregular Chiral Polymers. *Chem. Rev.* **2016**, *116*, 1094–1138.

(100) Kawauchi, T.; Kawauchi, M.; Kodama, Y.; Takeichi, T. Formation of the Inclusion Complex of Helical Syndiotactic

Poly(methyl methacrylate) and Polycyclic Aromatic Hydrocarbons. *Macromolecules* **2011**, *44*, 3452–3457.

(101) Shimomura, K.; Ikai, T.; Kanoh, S.; Yashima, E.; Maeda, K. Switchable Enantioseparation Based on Macromolecular Memory of a Helical Polyacetylene in the Solid State. *Nat. Chem.* **2014**, *6*, 429–434.

(102) Ishidate, R.; Sato, T.; Ikai, T.; Kanoh, S.; Yashima, E.; Maeda, K. Helicity Induction and Memory Effect in Poly(biphenylylacetylene)s Bearing Various Functional Groups and Their Use as Switchable Chiral Stationary Phases for HPLC. *Polym. Chem.* **2019**, *10*, 6260–6268.